

http://pubs.acs.org/journal/aelccp

Rapidly-Formed Interphase Facilitating Fast-Charging Lithium-Ion Batteries

Cong Zhong, Jiacheng Zhu, Xiaoyun Li, Suting Weng, Zhaoxiang Wang, Lifan Wang, Yejing Li, Chun Zhan,* and Xuefeng Wang*



Cite This: ACS Energy Lett. 2025, 10, 4627-4635



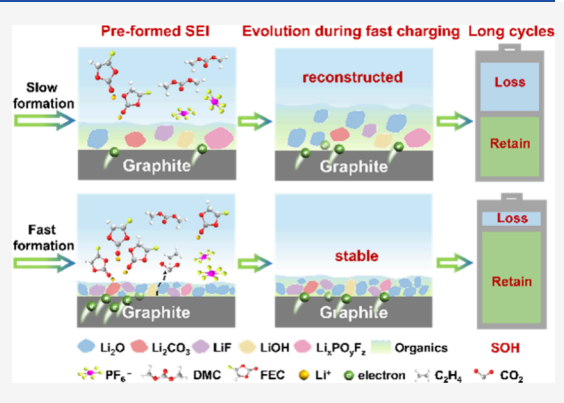
ACCESS I

III Metrics & More

Article Recommendations

Supporting Information

ABSTRACT: Sluggish lithium-ion (Li⁺) transport through the electrode–electrolyte interface hinders fast charging of lithium-ion batteries. Contrary to the conventionally slow-formed solid electrolyte interphase (SEI), fast-formed SEI is proposed and evidenced to be beneficial in enhancing the interfacial Li⁺ transport and thus the fast-charging of the graphite anode. Various characterization techniques including cryogenic transmission electron microscopy, in situ Raman spectroscopy, and gas chromatography are applied to uncover the nanostructure, formation pathways, and stability of SEI layers formed at varied current densities during the formation process. The results show that the rapidly formed SEI layer has more crystalline inorganic components with reduced size (4.4 nm at 5C vs. 8.0 nm at 0.2C), elevated stacking density (33% vs. 12%), thinner (~7 nm vs. 18 nm), and faster Li⁺ diffusion. With such a



preformed SEI layer, the capacity retention of the LiFePO₄||graphite cell is dramatically improved from 65% to 98% at 1C after 400 cycles.

he success of lithium-ion batteries (LIBs) relies greatly on the formation of a good passivating solid electrolyte interphase (SEI) layer at the electrode—electrolyte interface. To build a reliable SEI layer on the graphite anode, LIBs newly assembled are initially cycled with sophisticated conditions, typically at a low rate of <0.1C, to ensure a thick protection layer on the anode surface. Although the slow formation protocol is generally applied for current battery manufacture, it may not be the best prerequisite for batteries operating under different scenarios, such as fast charging.

The mass adoption of LIBs in electric vehicles demands fast-charging capability, achieving 80% state-of-charge (SOC) within 15 min.⁵ Fast charging is pretty convenient for consumers but remains challenging for the battery chemistry, especially for the relatively sluggish Li⁺ transport through the conventionally slow-formed SEI layer.^{6–8} The resistance of the SEI layer results in severe polarization, irreversible capacity loss, and Li metal plating when a high charging current is applied.^{9–11} Recently, rapid formation protocols have been used to enhance the fast-charging capacity and capacity retention.^{12–15} However, up to now, it has still been debated whether the higher formation rate is beneficial or harmful to facilitate fast-charging batteries.

To address the concerns regarding the rapid formation protocol, it is essential to identify the exact composition and morphology of the SEI layer formed at high rates. However, it remains a big challenge to quantitatively draw a clear picture of the inorganic—organic composite mosaic nanostructure of SEI formed at different rates, which is critical to the Li diffusion kinetics as well as the thermodynamical stability of the SEI. Yang found that the thickness of the SEI layer increases by approximately 10 nm after 2000 cycles at a low charging rate (0.5C) while its composition changes slightly. It is still unrevealed whether the SEI layer can withstand mechanical fracturing and thermal decomposition at a high rate. Therefore, it is critical to establish a comprehensive relationship for the SEI layer between fast kinetics and stable thermodynamics. 6,19,20

Herein, via quantitative identification of both the growth and the evolution of the SEI layer, we succeeded in establishing the correlation between the formation rate and the fast-charging durability of Li-ion batteries. A varied SEI layer was achieved by simply altering the current density during the formation process, and its Li⁺-transport capability was evaluated by the rate performance of the graphite anode. The composition and

Received: July 30, 2025 Revised: August 27, 2025 Accepted: August 28, 2025



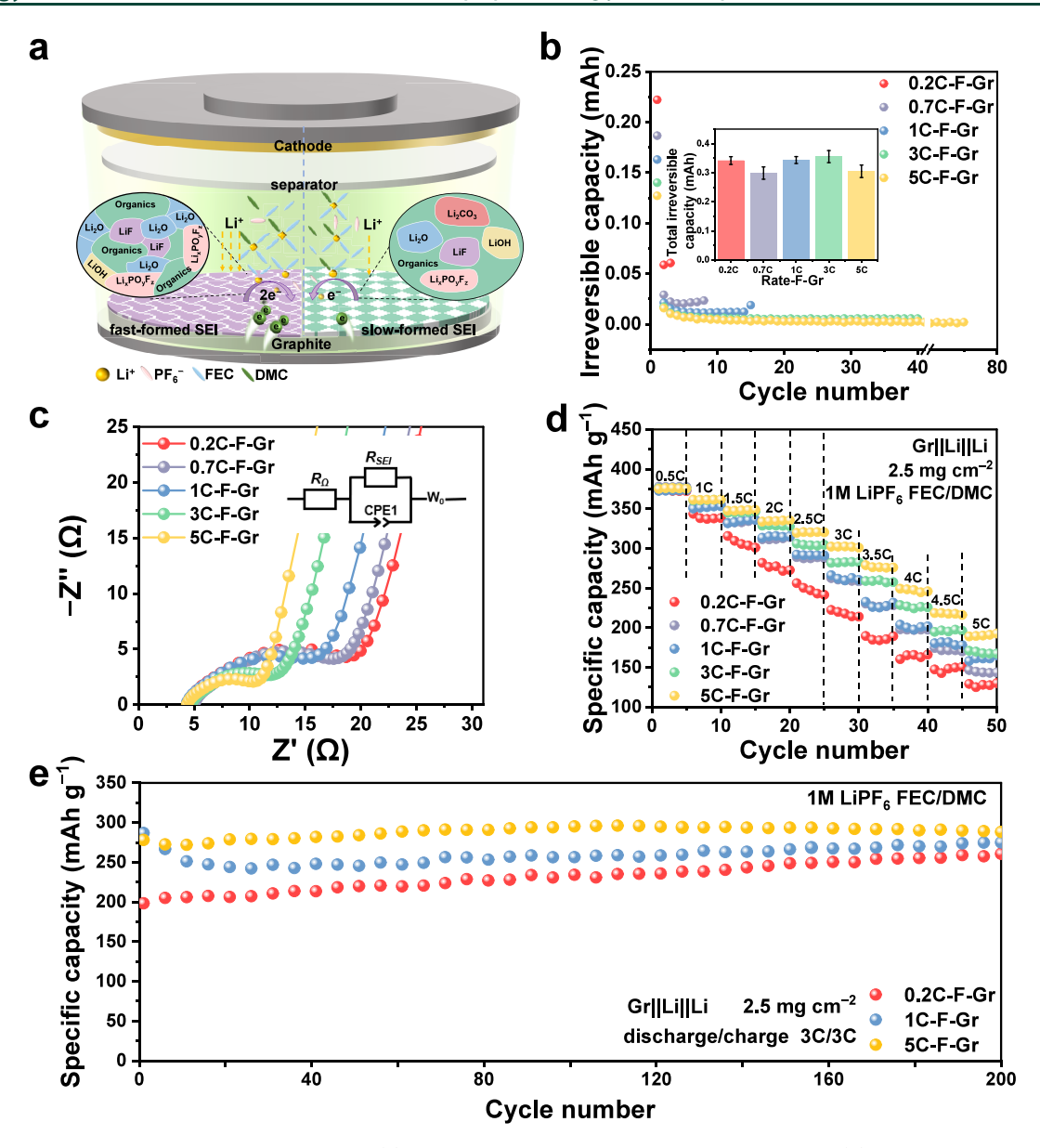


Figure 1. Rate-dependent SEI for the graphite anode. (a) Schematic for fast- and slow-formed interphase. (b) Irreversible capacity losses per cycle and total irreversible capacity losses (inset) during formation processes. (c) EIS spectra of Lillrate-F-Gr (rate = 0.2C, 0.7C, 1C, 3C, and 5C) cells. (d) Rate performances of the rate-F-Gr in three-electrode cells after formation processes. (e) Long-cycling performance at 3C of the rate-F-Gr (rate = 0.2C, 1C, and 5C). The same rate was used for each charge and discharge.

nanostructure of interphases were revealed by X-ray photoelectron spectroscopy (XPS), cryogenic transmission electron microscopy (cryo-TEM), and electron energy loss spectroscopy (EELS). The influence of current density on the electrolyte and its decomposition pathway has been probed by in situ Raman and gas chromatography (GC). It is found that higher current density facilitates formation of thinner (~7 nm at 5C vs. 18 nm at 0.2C) SEI layer rich in crystalline inorganics with reduced size (~4.4 nm vs. 8.0 nm) and increased stacking (33% vs. 12%), enhancing the Li⁺ transport through the SEI layer. Meanwhile, this rapidly formed SEI layer can maintain composition and structure stability during fast charging. These findings emphasize the essential role of interphase in regulating the battery reaction kinetics and stable dynamics and provide valuable guidelines for interface engineering without changing battery chemistry, thus further improving the sustainable lifespans of LIBs.

Changing the current density during the formation process is expected to tune the nanostructure of the SEI layer (Figure 1a). The three-electrode configuration enables precise graphite potential control (0-3 V vs. Li⁺/Li) while preventing metallic Li deposition (Figure S1). A fluoroethylene carbonate (FEC)based electrolyte was used since it shows better rate performance than the ethylene carbonate (EC) counterpart owing to its well-known film-formation capability (Figure S2).21,22 The cells were subjected to different formation conditions with similar irreversible capacity (Figure 1b, ~0.3 mAh) rather than identical cycle number (Figure S3) to form sufficient SEI by 0.2C (3 cycles), 0.7C (8 cycles), 1C (15 cycles), 3C (40 cycles), and 5C (75 cycles) (Figure S4a-g), yielding "rate-F-Gr" (e.g., 0.2C-F-Gr). Drastically increasing the current density from 0.2C to 5C increases the cell polarization for about 84 mV and thus less Li⁺ is intercalated into the graphite (Figure S4f,g). Electrochemical impedance

ACS Energy Letters http://pubs.acs.org/journal/aelccp Letter

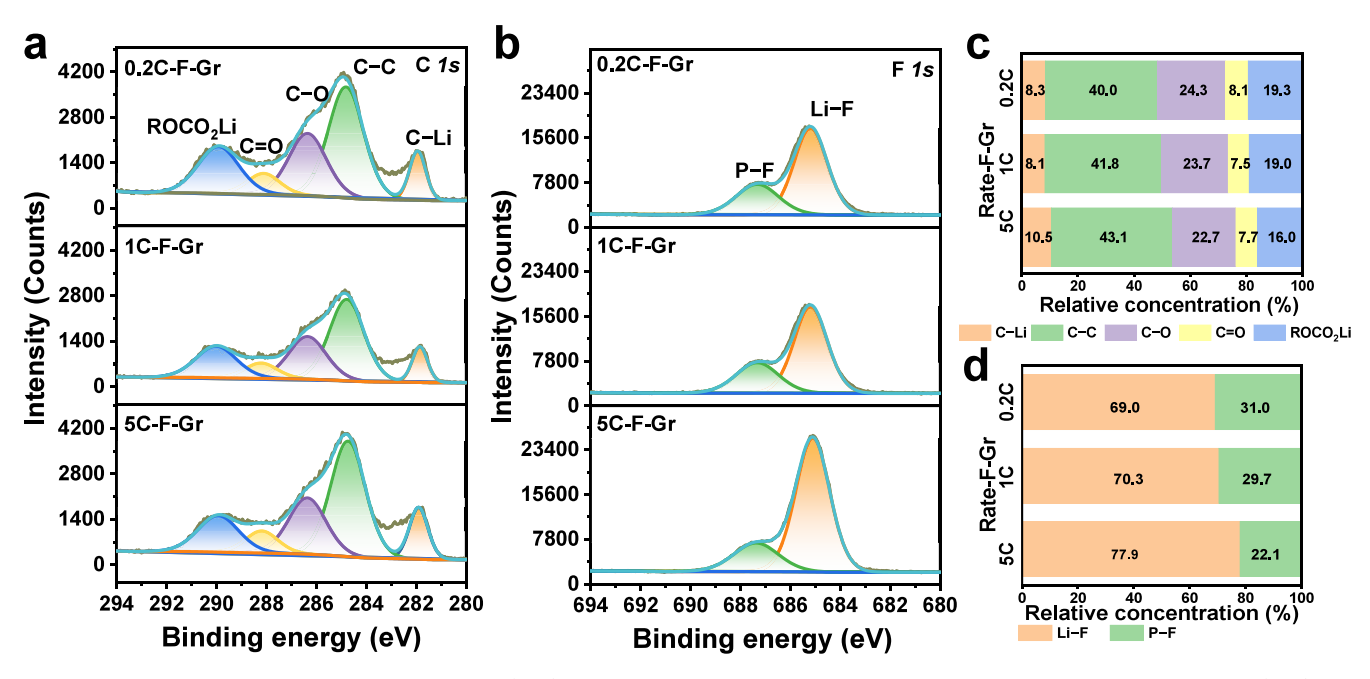


Figure 2. Interphase composition after formation. (a, b) XPS spectra of C 1s and F 1s from 0.2C-F-Gr, 1C-F-Gr, and 5C-F-Gr. (c, d) The relative atomic ratio of C-Li, C-C, C-O, C=O, and ROCO₂Li based on C 1s spectra (c) and Li-F, P-F based on F 1s spectra (d).

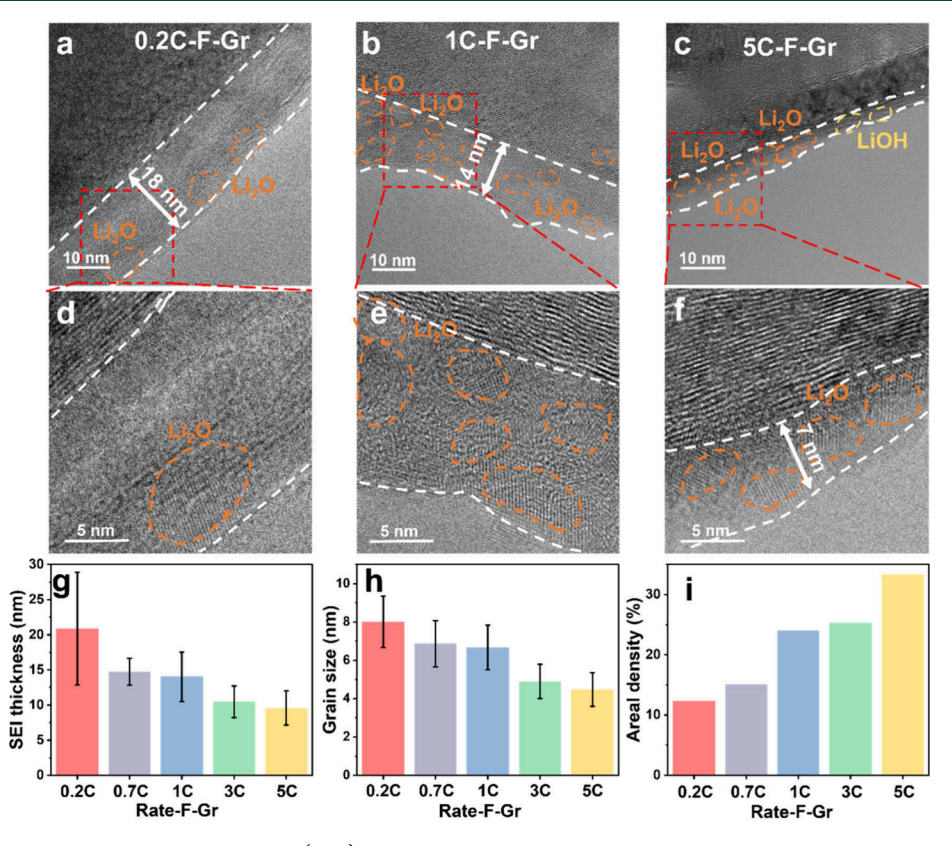


Figure 3. Interphase nanostructure after formation. (a-c) Cryo-TEM images of SEI layers of the 0.2C-F-Gr, 1C-F-Gr, and 5C-F-Gr. (d-f) The corresponding magnified regions of Figure 3a-c. (g) Statistical average SEI thickness based on TEM images. Error bars denote one standard deviation calculated from 15 images. (h) Statistical average grain size of crystalline inorganic nanograins $(Li_2O/LiOH/Li_2CO_3)$. Error bars denote one standard deviation calculated from 20 grains. (i) The statistical areal density of crystalline inorganics in the SEI. The areal density of crystalline inorganics was calculated by dividing the area of these crystalline inorganic nanograins by the overall area of the SEI layer (labeled by a white dashed line).

spectroscopy (EIS) measurements demonstrate that the 5C-F-Gr cell has the lowest interfacial resistance ($R_{SEI} = 4.4 \Omega$, Figure 1c and Table S1), and the 0.2C-F-Gr cell exhibits the

highest resistance ($R_{SEI} = 15.6 \Omega$).²³ The interfacial resistance indicates the varied Li⁺ conductivity of the SEI layer, which is related to its nanostructure.^{23,24}

ACS Energy Letters http://pubs.acs.org/journal/aelccp Letter

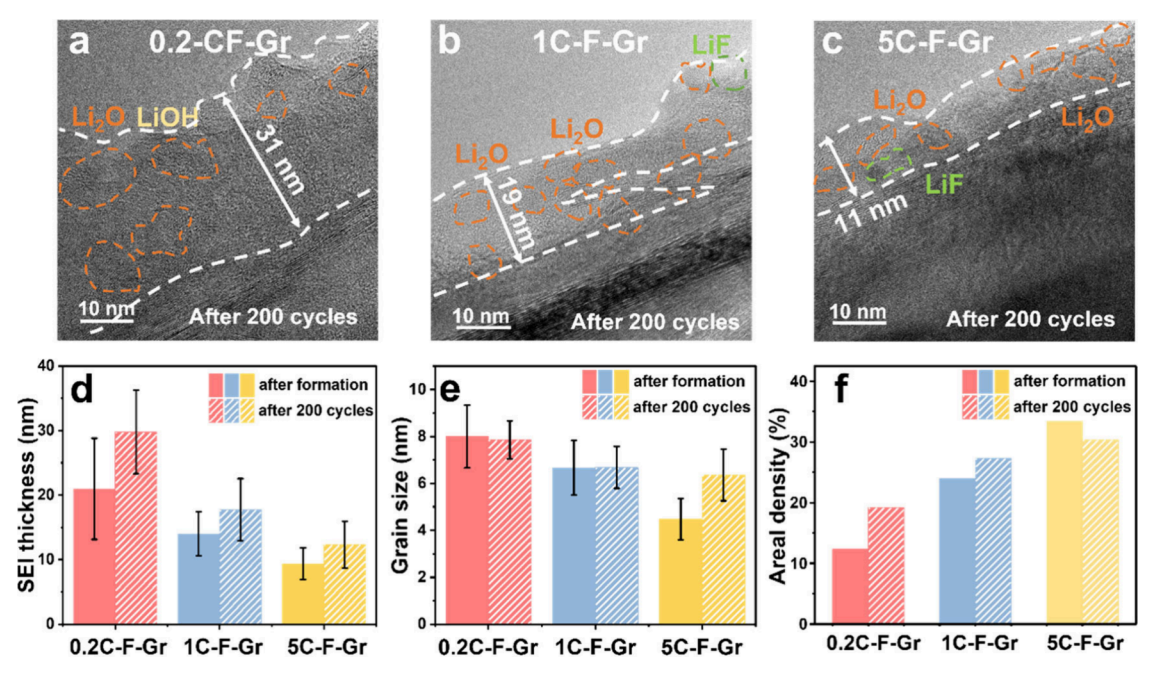


Figure 4. Interphase stability after cycling at 3C for 200 cycles. (a-c) Cryo-TEM images of SEI layers on 0.2C-F-Gr, 1C-F-Gr, and 5C-F-Gr. (d) SEI layer thickness changes, (e) grain size changes, (f) areal density of crystalline inorganics changes before and after 200 cycles. Error bars denote one standard deviation calculated from 15 images (d) and 20 grains (e).

To assess the Li⁺-transport capability of the as-prepared SEI layers, we evaluated and compared the rate performances of the graphite electrodes were evaluated and compared. Figure 1d and Figure S5 show that all of the graphite with high-rate formation displays better rate capacity than the 0.2C-F-Gr. Notably, the 5C-F-Gr delivers a capacity of 190 mAh g⁻¹ at 5C, while the 0.2C-F-Gr is 130 mAh g⁻¹. This suggests that the SEI layer formed under higher current density promotes faster Li⁺ transport, enhancing the fast-charging capability of the graphite anode. To further validate the benefits of the fast formation, the cycling performance was compared (Figure 1e) and the 5C-F-Gr displays a higher reversible capacity (288 mAh g⁻¹) than 1C-F-Gr (275 mAh g⁻¹) and 0.2C-F-Gr (269 mAh g⁻¹) after 200 cycles at 3C.

The nature of SEI layers formed at different rates was probed by XPS. Based on the XPS spectra (Figure 2 and Figure S6), the atomic ratio of C, Li, O, F, and P in SEI layers was determined, and a notably higher F relative concentration in the 5C-F-Gr (Figure S6b) indicates the intensified decomposition of F-containing solvent (FEC) or/and salt (LiPF₆) at the high rate. The latter is confirmed by the slightly higher P content in 5C-F-Gr (0.49% vs. 0.33% in 0.2C-F-Gr, Figure S6b). All the C 1s spectra (Figure 2a) can be decoupled into five peaks ascribed to ROCO₂Li (~289.8 eV), C=O (~288.6 eV), C-O (~286.4 eV), C-C (284.8 eV), and C-Li (282.0 eV).25-27 Despite a negligible difference in the chemical composition, the relative amounts of C-O, C=O, and ROCO₂Li decrease with increasing current density (Figure 2c), suggesting that the SEI layer formed at the lower current density has more organic components, potentially resulting in sluggish Li⁺ transport. 28,29 In addition, F 1s spectra shows Li_xPO_yF_z (687.3 eV) and LiF (685.2 eV, Figure 2b) species and 77.9% content of LiF are found in 5C-F-Gr (Figure 2d), which is believed to promote fast Li⁺ transport through the SEI layer.30

Cryo-TEM was employed to investigate the nanostructure and composition of SEI formed at different rates. Regardless of the current density, the SEI layers exhibit a mosaic-like structure where crystalline inorganic nanograins are embedded within an amorphous matrix (Figure 3a-f and Figures S7-S12). In the SEI layer formed at 0.2C, these small crystalline inorganic nanograins, averaging ~8.0 nm in size, are sparsely distributed in the amorphous substrate (Figure 3d) and its areal density is approximately 12% (Figure 3i). Increasing the formation rate from 0.2C to 5C is found to reduce the SEI thickness (from 18 to 7 nm, Figure 3g) and decrease the grain size (from 8.0 to 4.4 nm) but increase the stacking density (from 33% to 12%) of the crystalline grains (Figure 3h,i). Although crystalline Li₂O exhibits a high Li⁺ diffusion barrier, its Li₂O/Li₂O nanograin boundaries are expected to serve as effective pathways for Li⁺ transport,³¹ thereby reducing interfacial impedance and enabling superior electrochemical performance of the graphite anode.

Through EELS spectra, the presence of Li_2O as a dominating inorganic component in the SEI layer is confirmed (Figure S13a). A prominent peak at 301 eV in the C K-edge spectrum (Figure S13b) suggests a greater diversity of organic species on the surface of 0.2C-F-Gr, which agrees with the cryo-TEM observation (Figure 3d) and XPS results (Figure 2a).

To assess SEI dynamic stability, these rate-F-Grs were cycled at 3C for 200 cycles (Figure 4a–c, Figures S14–16). Compared to the SEI initially formed at 0.2C on the graphite, the SEI after subsequent 200 cycles at 3C has more crystalline inorganic components (Figure 4a,f) and increased thickness (from 18 to 31 nm, Figure 4d). This evolution demonstrates that the slowly formed SEI undergoes reconstruction and growth during the subsequent 3C cycling. This evolution is potentially due to the thermodynamically unstable organics 32–34 and Joule heat. 32,35 The damaged SEI layer allows the electrolyte to permeate the SEI layer, which promotes the

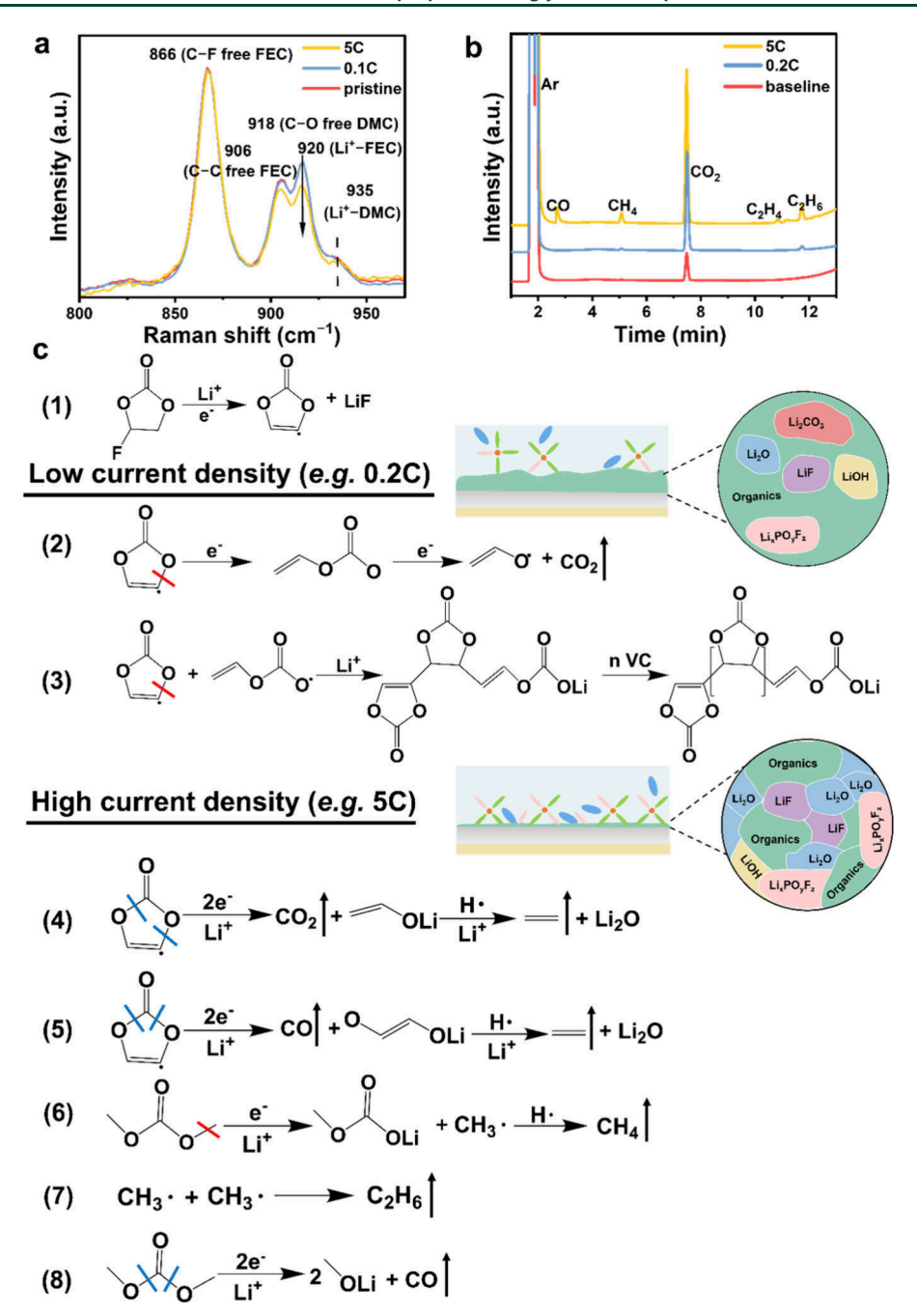


Figure 5. Formation mechanism of SEI layers at different rates. (a) In situ Raman spectra of the electrolyte near the graphite anode at different current densities. (b) GC spectra obtained from the gases released at 0.2C and 5C. The detected CO₂ in the baseline is from the glovebox. (c) The potential pathways for the decomposition of FEC and DMC at different current densities.

reformation of the SEI layer in the subsequent cycling.³⁶ In contrast, the SEI layers formed at 1C and 5C maintain pristine structure (Figure 4b,c) and slightly increase in thickness (~19 nm on 1C-F-Gr, and ~11 nm on 5C-F-Gr) after 200 cycles at 3C (Figure 4d-f), which reveals that, albeit thin, the rapidly prepared SEI layer is evidenced to be relatively compact and stable during fast charging. These results are consistent with the computational results, which demonstrated that a high ionic conductivity of the SEI enhances interfacial stability.³⁷

The distinct SEI structures suggest that electrolyte reaction mechanisms vary with current density. To probe the electrolyte change under different rates, *in situ* Raman spectroscopic measurement (Figure S17) was performed. At 0.1C, the

Raman spectra of the electrolyte are almost identical to the original one, showing peaks for free DMC molecules (918 cm⁻¹), ³⁸ Li⁺ bonded to DMC molecules (Li⁺–DMC, at 935 cm⁻¹), free FEC molecules (906 cm⁻¹), and Li⁺ bonded to FEC (Li⁺–FEC, at 920 cm⁻¹, Figure 5a and Figure S17d). When at 5C, Li⁺–solvent peak intensities (especially Li⁺–FEC at 920 cm⁻¹; Figure S18) decrease relative to free solvents, indicating the rapid consumption of Li⁺–solvent complexes for SEI formation.

The accompanying gas evolution during SEI layer formation was monitored by GC (Figure 5b and Figure S19). Notably, CO_2 is dominantly detected at 0.2C, while CO_2 , CO_3 , CO_4 , CO_2 , and CO_3 are present at CO_4 , implying varied reaction

ACS Energy Letters http://pubs.acs.org/journal/aelccp Letter

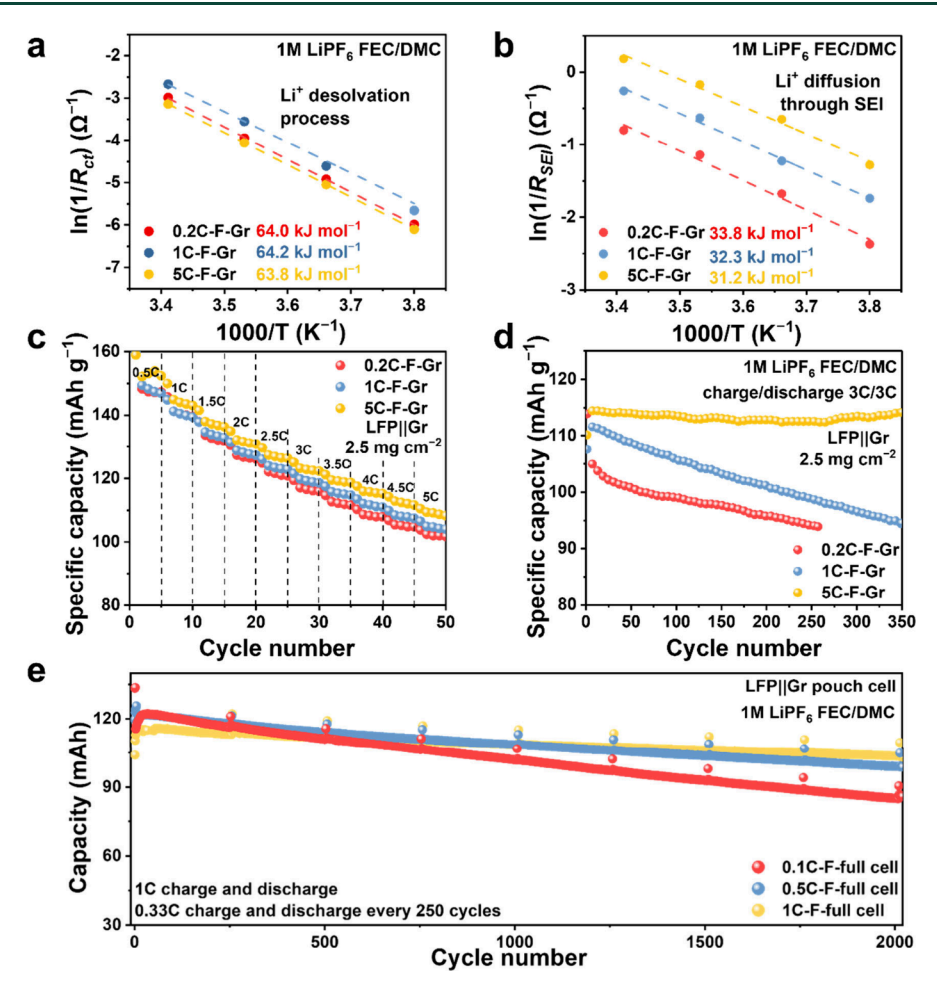


Figure 6. Electrochemical performance of graphite anode with rate-dependent SEI layer. (a, b) Activation energies related to Li⁺ desolvation (a) and Li⁺ diffusion through the SEI layer (b) for Lillrate-F-Gr (rate = 0.2C, 1C, and 5C) cell in the 1 M LiPF₆ FEC/DMC electrolyte calculated using the Arrhenius equation based on the fitted resistance from -10 to 20 °C. (c, d) Rate performances (c) and long-cycling performances (d) of LFP||rate-F-Gr (rate = 0.2C, 1C, and 5C) full cells with graphite loading of 2.5 mg cm⁻². (e) Long-cycling performances of LFP||Gr pouch cells at 1C after preformation at 0.1C, 0.5C, and 1C for three cycles.

pathways dependent on the current density (Figure 5c). Specifically, FEC is initially reduced to form VC radicals and LiF (reaction (1)). At this low rate, VC radicals are likely further reduced and recombined into poly-VC, releasing CO_2 through reactions (2) and (3). In contrast, two C–O bonds in the VC radicals may undergo cleavage (illustrated by blue lines in reactions (4) and (5)) and further decompose into Li₂O, CO_2 , CO, and C_2H_4 at a high rate. Consequently, a series of gases is released, and the SEI layer formed at a higher rate has more inorganic components. The formation of CH_4 and C_2H_6 is attributed to the cleavage of the C–O bond in the DMC (reactions (6) and (7)). 39,40 Additionally, the cleavage of two C–O bonds in DMC (labeled by the blue line, reaction (8)) may also occur and generate CO.

Elevated current densities enhance the chemical reactions and induce a higher overpotential at the graphite anode, which alters the thermodynamic pathway, suppressing the polymerization of organic solvents (e.g., FEC) while promoting inorganic species formation (e.g., LiOH, Li₂O, Li₂CO₃), leading to an inorganic-rich, thin SEI layer (<10 nm). The grain size of inorganics follows a classical nucleation mechanism (eq 1)⁴¹

$$r = \frac{2\gamma V_m}{F\eta} \tag{1}$$

where r is the critical radius, γ is the surface energy of the SEI, V_m is the molar volume of inorganics, F is Faraday's constant, and η is overpotential. The critical radius (r) is inversely related to overpotential (η) . 42,43 In addition, the elevated current density accelerates electrolyte reduction and depletes surface Li⁺, establishing diffusion-limited conditions, which inhibit the growth of grains, resulting in a dense SEI structure with small inorganic grains, the compact structure of which effectively suppresses electrolyte decomposition and maintains interfacial stability during fast charging.

The aforementioned rate-dependent interphases provide a feasible and ingenious approach to distinguish the processes from Li⁺ transport through the SEI layer and desolvation in the same electrolyte in determining the rate-limiting reaction steps in the batteries. To experimentally separate them and estimate their activation energy, temperature-dependent EIS was conducted on "Lillrate-F-Gr" cells, and the resistance for the charge transfer (R_{ct}) and Li⁺ transport through the SEI layer (R_{SEI}) were fitted as a function of temperature (Figure S20 and Table S2). Based on the Arrhenius equation (eq 2)^{44,45}

$$\frac{1}{R_{ct}} = Ae^{-E_a/RT} \tag{2}$$

the activation energy (E_a) for the desolvation process was calculated to be 64.0 kJ mol⁻¹ for 0.2C-F-Gr, 64.2 kJ mol⁻¹ for 1C-F-Gr, and 63.8 kJ mol⁻¹ for 5C-F-Gr (Figure 6a); the close values suggest that the desolvation process is mainly dependent on the electrolyte chemistry rather than the SEI layer.^{7,46} In addition, the E_a for Li⁺ diffusion in the SEI layer was determined to be 33.8 kJ mol⁻¹ for 0.2C-F-Gr, 32.3 kJ mol⁻¹ for 1C-F-Gr, and 31.2 kJ mol⁻¹ for 5C-F-Gr (Figure 6b), demonstrating the faster Li⁺ transport capability of the rapidly formed SEI layer. This merit becomes more obvious in the EC-based electrolyte (1 M LiPF₆ EC/DMC), in which the E_a for Li⁺ diffusion in the SEI layer was determined to be 44.6 kJ mol⁻¹ for 0.2C-F-Gr and 21.3 kJ mol⁻¹ for 5C-F-Gr (Figure S21 and Table S3).

The benefit of the fast-preformed SEI layer is also present in the LiFePO₄ (LFP)llrate-F-Gr full cells (Figure 6c and Figure S22). The cell with 5C-F-Gr as the anode delivers a rate capacity higher than those with 0.2C-F-Gr and 1C-F-Gr (Figure 6c), consistent with the three-electrode cell results (Figure 1d). After 250 cycles at 3C, the capacity of LFPIISC-F-Gr is 113 mAh g⁻¹ while those of LFP||1C-F-Gr and LFP|| 0.2C-F-Gr are 98 mAh g⁻¹ and 93 mAh g⁻¹, respectively (Figure 6d). For pouch cells (134 mAh), 1C was used during the rapid formation process to prevent the potential Li deposition caused by the localized high current densities (>1C).47 The 1C-F-full cell and 0.5C-F-full cell deliver 110 mAh and 105 mAh, remaining 82% capacity and 78% after 2000 cycles, respectively (Figure 6e), while the 0.1C-F-full cell retains 67%. These results demonstrate that the SEI layer derived from higher current density is indeed beneficial for fast interfacial Li⁺ transport and improving the rate and cycling performance of LIBs. This strategy is universal and has been proven to be effective with the commercial electrolyte 1 M LiPF₆ EC/DMC (Figures S23–S28).

In summary, clear pictures of the SEI layer formed at different current densities are intuitively observed (Figure 1a), showing that high current density can lead to favorable SEI nanostructures, reduce inorganics size (~4.4 nm), and increase stacking (33%), resulting in enhanced rate performance of graphite. The abundant inorganic interphase notably facilitates Li⁺ diffusion within the SEI layer and suppresses the continuous reaction between Gr and the electrolyte, prolonging the lifespan of the battery and enhancing its Coulombic efficiencies. These findings establish a direct correlation between interphase nanostructure, fast-charging kinetics, and long-term cycling stability, offering an actionable design strategy for sustainable, high-performance LIBs.

ASSOCIATED CONTENT

Supporting Information

The Supporting Information is available free of charge at https://pubs.acs.org/doi/10.1021/acsenergylett.5c02398.

Experimental methods (including electrolyte, electrochemical measurement, characterizations), additional electrochemical data and images, additional XPS data, tables of EIS fitting results, additional TEM images, and additional Raman spectra data (PDF)

AUTHOR INFORMATION

Corresponding Authors

Xuefeng Wang — Beijing National Laboratory for Condensed Matter Physics, Institute of Physics, Chinese Academy of Sciences, Beijing 100190, China; College of Materials Science and Optoelectronic Technology, University of Chinese Academy of Sciences, Beijing 100049, China; ◎ orcid.org/0000-0001-9666-8942; Email: wxf@iphy.ac.cn

Chun Zhan — State Key Laboratory of Advanced Metallurgy, School of Metallurgical and Ecological Engineering, University of Science and Technology Beijing, Beijing 100083, China; Department of Energy Storage Science and Engineering, School of Metallurgical and Ecological Engineering, University of Science and Technology Beijing, Beijing 100083, China; orcid.org/0000-0002-6360-2514; Email: zhanchun@ustb.edu.cn

Authors

Cong Zhong — Beijing National Laboratory for Condensed Matter Physics, Institute of Physics, Chinese Academy of Sciences, Beijing 100190, China; State Key Laboratory of Advanced Metallurgy, School of Metallurgical and Ecological Engineering, University of Science and Technology Beijing, Beijing 100083, China; Department of Energy Storage Science and Engineering, School of Metallurgical and Ecological Engineering, University of Science and Technology Beijing, Beijing 100083, China

Jiacheng Zhu — Beijing National Laboratory for Condensed Matter Physics, Institute of Physics, Chinese Academy of Sciences, Beijing 100190, China; College of Materials Science and Optoelectronic Technology, University of Chinese Academy of Sciences, Beijing 100049, China

Xiaoyun Li — Beijing National Laboratory for Condensed Matter Physics, Institute of Physics, Chinese Academy of Sciences, Beijing 100190, China

Suting Weng – Beijing National Laboratory for Condensed Matter Physics, Institute of Physics, Chinese Academy of Sciences, Beijing 100190, China

Zhaoxiang Wang — Beijing National Laboratory for Condensed Matter Physics, Institute of Physics, Chinese Academy of Sciences, Beijing 100190, China; College of Materials Science and Optoelectronic Technology, University of Chinese Academy of Sciences, Beijing 100049, China; orcid.org/0000-0002-1123-6591

Lifan Wang — State Key Laboratory of Advanced Metallurgy, School of Metallurgical and Ecological Engineering, University of Science and Technology Beijing, Beijing 100083, China; Department of Energy Storage Science and Engineering, School of Metallurgical and Ecological Engineering, University of Science and Technology Beijing, Beijing 100083, China; orcid.org/0000-0002-8426-434X

Yejing Li — Beijing National Laboratory for Condensed Matter Physics, Institute of Physics, Chinese Academy of Sciences, Beijing 100190, China; State Key Laboratory of Advanced Metallurgy, School of Metallurgical and Ecological Engineering, University of Science and Technology Beijing, Beijing 100083, China

Complete contact information is available at: https://pubs.acs.org/10.1021/acsenergylett.5c02398

Author Contributions

C. Zhong, X.W., and C. Zhan conceived the idea and designed the project. J.Z. conducted *in situ* Raman spectroscopy and GC test. X.L. performed XPS measurements. C. Zhong performed all the other data collection and analysis. X.L., S.W., Z.W., L.W., and Y.L. contributed to discussions and interpretation of results. C. Zhong, X.W., and C. Zhan cowrote the manuscript, with input from all authors.

Notes

The authors declare no competing financial interest.

ACKNOWLEDGMENTS

This work was supported by the National Key R&D Program of China (Grant Nos.2022YFB2502200 and 2021YFC2900900), the National Natural Science Foundation of China (NSFC Nos.52172257, 521002206, and 22409211), the China Postdoctoral Science Foundation (No. 2023M743739), and the Postdoctoral Fellowship Program of CPSF (No. GZC20232939).

REFERENCES

- (1) Peled, E. The Electrochemical Behavior of Alkali and Alkaline Earth Metals in Nonaqueous Battery Systems-The Solid Electrolyte Interphase Model. *J. Electrochem. Soc.* **1979**, *126* (12), 2047–2051.
- (2) Winter, M.; Barnett, B.; Xu, K. Before Li Ion Batteries. Chem. Rev. 2018, 118 (23), 11433-11456.
- (3) Wood, D. L.; Li, J.; Daniel, C. Prospects for reducing the processing cost of lithium ion batteries. *J. Power Sources* **2015**, 275, 234–242
- (4) Peled, E.; Menkin, S. Review—SEI: Past, Present and Future. J. Electrochem. Soc. 2017, 164 (7), A1703-A1719.
- (5) Ahmed, S.; Bloom, I.; Jansen, A. N.; Tanim, T.; Dufek, E. J.; Pesaran, A.; Burnham, A.; Carlson, R. B.; Dias, F.; Hardy, K.; et al. Enabling fast charging-A battery technology gap assessment. *J. Power Sources* **2017**, *367*, 250–262.
- (6) Tan, J.; Matz, J.; Dong, P.; Shen, J.; Ye, M. A Growing Appreciation for the Role of LiF in the Solid Electrolyte Interphase. *Adv. Energy Mater.* **2021**, *11* (16), 2100046.
- (7) Weng, S.; Zhang, X.; Yang, G.; Zhang, S.; Ma, B.; Liu, Q.; Liu, Y.; Peng, C.; Chen, H.; Yu, H.; et al. Temperature-dependent interphase formation and Li⁺ transport in lithium metal batteries. *Nat. Commun.* **2023**, *14* (1), 4474.
- (8) McShane, E. J.; Colclasure, A. M.; Brown, D. E.; Konz, Z. M.; Smith, K.; McCloskey, B. D. Quantification of Inactive Lithium and Solid-Electrolyte Interphase Species on Graphite Electrodes after Fast Charging. ACS Energy Lett. 2020, 5 (6), 2045–2051.
- (9) Cai, W.; Yao, Y. X.; Zhu, G. L.; Yan, C.; Jiang, L. L.; He, C.; Huang, J. Q.; Zhang, Q. A review on energy chemistry of fast-charging anodes. *Chem. Soc. Rev.* **2020**, *49* (12), 3806–3833.
- (10) Weiss, M.; Ruess, R.; Kasnatscheew, J.; Levartovsky, Y.; Levy, N. R.; Minnmann, P.; Stolz, L.; Waldmann, T.; Wohlfahrt-Mehrens, M.; Aurbach, D.; et al. Fast Charging of Lithium-Ion Batteries: A Review of Materials Aspects. *Adv. Energy Mater.* **2021**, *11* (33), 2101126.
- (11) Li, W. Onset of Lithium Plating in Fast-Charging Li-Ion Batteries. ACS Energy Lett. 2025, 10 (4), 1596–1604.
- (12) Weng, A.; Mohtat, P.; Attia, P. M.; Sulzer, V.; Lee, S.; Less, G.; Stefanopoulou, A. Predicting the impact of formation protocols on battery lifetime immediately after manufacturing. *Joule* **2021**, *5* (11), 2971–2992.
- (13) An, S. J.; Li, J.; Du, Z.; Daniel, C.; Wood, D. L. Fast formation cycling for lithium ion batteries. *J. Power Sources* **2017**, 342, 846–852. (14) Cui, X.; Kang, S. D.; Wang, S.; Rose, J. A.; Lian, H.; Geslin, A.;
- (14) Cui, X.; Kang, S. D.; Wang, S.; Rose, J. A.; Lian, H.; Geslin, A.; Torrisi, S. B.; Bazant, M. Z.; Sun, S.; Chueh, W. C. Data-driven analysis of battery formation reveals the role of electrode utilization in extending cycle life. *Joule* **2024**, *8* (11), 3072–3087.

- (15) Kim, S.; Didwal, P. N.; Fiates, J.; Dawson, J. A.; Weatherup, R. S.; De Volder, M. Effect of the Formation Rate on the Stability of Anode-Free Lithium Metal Batteries. *ACS Energy Lett.* **2024**, 9 (10), 4753–4760.
- (16) Zhang, H.; Peng, Y.; Hu, Y.; Pan, S.; Tang, S.; Luo, Y.; Liang, Y.; Liao, Y.; Lin, Y.; Zhang, K.; et al. Quantitative Analysis of Aging and Rollover Failure Mechanisms of Lithium-Ion Batteries at Accelerated Aging Conditions. *Adv. Energy Mater.* **2025**, *15* (19), 2404997.
- (17) Sarkar, A.; Shrotriya, P.; Nlebedim, I. C. Anodic Interfacial Evolution in Extremely Fast Charged Lithium-Ion Batteries. *ACS Applied Energy Materials* **2022**, *5* (3), 3179–3188.
- (18) Tomaszewska, A.; Chu, Z.; Feng, X.; O'Kane, S.; Liu, X.; Chen, J.; Ji, C.; Endler, E.; Li, R.; Liu, L.; et al. Lithium-ion battery fast charging: A review. *eTransportation* **2019**, *1*, 100011.
- (19) Kranz, S.; Kranz, T.; Jaegermann, A. G.; Roling, B. Is the solid electrolyte interphase in lithium-ion batteries really a solid electrolyte? Transport experiments on lithium bis(oxalato)borate-based model interphases. *J. Power Sources* **2019**, *418*, 138–146.
- (20) Yu, Y.; Koh, H.; Zhang, Z.; Yang, Z.; Alexandrova, A. N.; Agarwal, M.; Stach, E. A.; Xie, J. Kinetic pathways of fast lithium transport in solid electrolyte interphases with discrete inorganic components. *Energy Environ. Sci.* 2023, *16*, 5904–5915.
- (21) Huang, W.; Attia, P. M.; Wang, H.; Renfrew, S. E.; Jin, N.; Das, S.; Zhang, Z.; Boyle, D. T.; Li, Y.; Bazant, M. Z.; et al. Evolution of the Solid-Electrolyte Interphase on Carbonaceous Anodes Visualized by Atomic-Resolution Cryogenic Electron Microscopy. *Nano Lett.* **2019**, *19* (8), 5140–5148.
- (22) Dong, Y.; Chen, Y.; Yue, X.; Liang, Z. Unveiling the adsorption tendency of film-forming additives to enable fast-charging hard carbon anodes with regulated Li plating. *Energy Environ. Sci.* **2024**, *17* (7), 2500–2511.
- (23) Kranz, S.; Kranz, T.; Graubner, T.; Yusim, Y.; Hellweg, L.; Roling, B. Influence of the Formation Current Density on the Transport Properties of Galvanostatically Formed Model-Type Solid Electrolyte Interphases. *Batteries & Supercaps* **2019**, 2 (12), 1026–1036.
- (24) Zhang, S.; Li, Y.; Bannenberg, L. J.; Liu, M.; Ganapathy, S.; Wagemaker, M. The lasting impact of formation cycling on the Li-ion kinetics between SEI and the Li-metal anode and its correlation with efficiency. *Sci. Adv.* **2024**, *10*, No. eadj8889.
- (25) Agubra, V. A.; Fergus, J. W. The formation and stability of the solid electrolyte interface on the graphite anode. *J. Power Sources* **2014**, 268, 153–162.
- (26) Ota, H.; Sakata, Y.; Inoue, A.; Yamaguchi, S. Analysis of Vinylene Carbonate Derived SEI Layers on Graphite Anode. *J. Electrochem. Soc.* **2004**, *151* (10), A1659–A1669.
- (27) Hellqvist Kjell, M.; Malmgren, S.; Ciosek, K.; Behm, M.; Edström, K.; Lindbergh, G. Comparing aging of graphite/LiFePO₄ cells at 22 and 55 $^{\circ}$ C Electrochemical and photoelectron spectroscopy studies. *J. Power Sources* **2013**, 243, 290–298.
- (28) Lei, S.; Zeng, Z.; Liu, M.; Zhang, H.; Cheng, S.; Xie, J. Balanced solvation/de-solvation of electrolyte facilitates Li-ion intercalation for fast charging and low-temperature Li-ion batteries. *Nano Energy* **2022**, *98*, 107265.
- (29) Zhang, S.; Yang, G.; Liu, S.; Li, X.; Wang, X.; Wang, Z.; Chen, L. Understanding the dropping of lithium plating potential in carbonate electrolyte. *Nano Energy* **2020**, *70*, 104486.
- (30) Han, X.; Sun, J. Design of a LiF-rich solid electrolyte interface layer through salt-additive chemistry for boosting fast-charging phosphorus-based lithium ion battery performance. *Chem. Commun.* **2020**, *56* (45), 6047–6049.
- (31) Ramasubramanian, A.; Yurkiv, V.; Foroozan, T.; Ragone, M.; Shahbazian-Yassar, R.; Mashayek, F. Lithium Diffusion Mechanism through Solid-Electrolyte Interphase in Rechargeable Lithium Batteries. *J. Chem. Phys.* **2019**, *123* (16), 10237–10245.
- (32) Wu, J.; Weng, S.; Zhang, X.; Sun, W.; Wu, W.; Wang, Q.; Yu, X.; Chen, L.; Wang, Z.; Wang, X. In Situ Detecting Thermal Stability

- of Solid Electrolyte Interphase (SEI). Small 2023, 19 (25), No. e2208239.
- (33) Sun, S. Y.; Yao, N.; Jin, C. B.; Xie, J.; Li, X. Y.; Zhou, M. Y.; Chen, X.; Li, B. Q.; Zhang, X. Q.; Zhang, Q. The Crucial Role of Electrode Potential of a Working Anode in Dictating the Structural Evolution of Solid Electrolyte Interphase. *Angew. Chem., Int. Ed.* **2022**, *61* (42), No. e202208743.
- (34) McShane, E. J.; Bergstrom, H. K.; Weddle, P. J.; Brown, D. E.; Colclasure, A. M.; McCloskey, B. D. Quantifying Graphite Solid-Electrolyte Interphase Chemistry and its Impact on Fast Charging. *ACS Energy Lett.* **2022**, *7* (8), 2734–2744.
- (35) Oh, S. M.; Song, J.; Lee, S.; Jang, I.-C. Effect of current rate on the formation of the solid electrolyte interphase layer at the graphite anode in lithium-ion batteries. *Electrochim. Acta* **2021**, 397, 139269.
- (36) Tang, S.; Liang, Y.; Zhong, C.; Peng, Y.; Hu, Y.; Hu, W.; Liao, Y.; Lin, J.; Yang, X.; Zhang, H.; et al. Revisiting the Overdischarge Process as a Novel Accelerated Aging Method for LiFePO₄/Graphite Batteries through the Unveiling of SEI Evolution Mechanism. *Energy Stor. Mater.* **2025**, *74*, 103916.
- (37) Li, W.; Korbitz, W.; Tchelepi, H. A.; Tran, A. SEI-Electrolyte Dyads for Dendrite Suppression in Li-Metal Batteries. *J. Electrochem. Soc.* **2025**, *172* (7), 070524.
- (38) Song, G.; Yi, Z.; Su, F.; Xie, L.; Wang, Z.; Wei, X.-X.; Xu, G.; Chen, C.-M. Boosting the Low-Temperature Performance for Li-Ion Batteries in LiPF₆-Based Local High-Concentration Electrolyte. *ACS Energy Lett.* **2023**, 8 (3), 1336–1343.
- (39) Xu, K. Whether EC and PC Differ in Interphasial Chemistry on Graphitic Anode and How. *J. Electrochem. Soc.* **2009**, *156* (9), A751–A755.
- (40) Ma, B.; Sun, Q.; Wu, J.; Gu, X.; Yang, H.; Xie, M.; Liu, Y.; Cheng, T. Interfacial polymerization mechanisms assisted flame retardancy process of low-flammable electrolytes on lithium anode. *J. Colloid Interface Sci.* **2024**, *660*, 545–554.
- (41) Yao, Y. X.; Wan, J.; Liang, N. Y.; Yan, C.; Wen, R.; Zhang, Q. Nucleation and Growth Mode of Solid Electrolyte Interphase in Li-Ion Batteries. *J. Am. Chem. Soc.* **2023**, *145* (14), 8001–8006.
- (42) Pei, A.; Zheng, G.; Shi, F.; Li, Y.; Cui, Y. Nanoscale Nucleation and Growth of Electrodeposited Lithium Metal. *Nano Lett.* **2017**, *17* (2), 1132–1139.
- (43) Liu, X.; Wang, G.; Lv, Z.; Du, A.; Dong, S.; Cui, G. A Perspective on Uniform Plating Behavior of Mg Metal Anode: Diffusion Limited Theory versus Nucleation Theory. *Adv. Mater.* **2024**, *36* (9), 2306395.
- (44) Wang, Z.; Sun, Z.; Shi, Y.; Qi, F.; Gao, X.; Yang, H.; Cheng, H. M.; Li, F. Ion-Dipole Chemistry Drives Rapid Evolution of Li Ions Solvation Sheath in Low-Temperature Li Batteries. *Adv. Energy Mater.* **2021**, *11* (28), 2100935.
- (45) Yao, Y.-X.; Chen, X.; Yan, C.; Zhang, X.-Q.; Cai, W.-L.; Huang, J.-Q.; Zhang, Q. Regulating Interfacial Chemistry in Lithium-Ion Batteries by a Weakly Solvating Electrolyte. *Angew. Chem., Int. Ed.* **2021**, *60* (8), 4090–4097.
- (46) Jin, C. B.; Yao, N.; Xiao, Y.; Xie, J.; Li, Z.; Chen, X.; Li, B. Q.; Zhang, X. Q.; Huang, J. Q.; Zhang, Q. Taming Solvent-Solute Interaction Accelerates Interfacial Kinetics in Low-Temperature Lithium-Metal Batteries. *Adv. Mater.* **2023**, *35* (3), 202208340.
- (47) Peng, Y.; Ding, M.; Zhang, K.; Zhang, H.; Hu, Y.; Lin, Y.; Hu, W.; Liao, Y.; Tang, S.; Liang, J.; et al. Quantitative Analysis of the Coupled Mechanisms of Lithium Plating, SEI Growth, and Electrolyte Decomposition in Fast Charging Battery. ACS Energy Lett. 2024, 9 (12), 6022–6028.